Automated Detection of Type II Focal Cortical Dysplasia Guided by Low-Density Electroencephalogram

Ruifeng Zheng[1], Cong Chen[2,*], Lingqi Ye[2], Shuang Wang[2], Haibin Shen[1] and Kejie Huang[1,*]

[1]College of Information Science and Electronic Engineering, Zhejiang University, Hangzhou, China
[2]Department of Neurology and Epilepsy Center, The Second Affiliated Hospital, Zhejiang University School of Medicine, Hangzhou, China

Abstract

Focal cortical dysplasia (FCD) is a common etiology of drug-resistant focal epilepsy. MRI and positron emission tomography (PET) data have been routinely used in many epilepsy centers to identify FCD, and, in recent years, several automatic FCD detection methods combining MRI and PET data enhanced detection performance. Nevertheless, manually or automatically identifying FCD lesions with subtle structural features or of tiny sizes accurately remains a challenge. On the other hand, researches incorporating low-density electroencephalogram (EEG) data into automatic FCD detection are scarce. In this study, we propose a multi-modality solution which utilizes an extra modality derived from EEG to guide the detection of type II FCD. Firstly, an automatic FCD detection algorithm taking MRI and PET data as inputs was adopted to conduct preliminary FCD detection. Secondly, we employed low-density EEG data to estimate the approximate sources of interictal epileptiform discharges (IED) with an electrophysiological source imaging network. Subsequently, the preliminary FCD detection results were filtered or guided by the IED source imaging results. By combining low-density EEG data with MRI and PET data, our solution aims to improve FCD detection performance, especially among cases with weak structural and metabolic features.

Keywords

focal cortical dysplasia, electroencephalogram, electrophysiological source imaging,

1. Introduction

Focal cortical dysplasia (FCD) is one of the leading causes of drug-resistant epilepsy [1]. Surgical resection is the most effective approach to control epilepsy caused by FCD, and the success of surgery relies on accurately detecting the epileptogenic lesions during presurgical evaluations. However, FCD lesions often hide at the bottom of cortical sulci, making visual detection on MRI time-consuming and highly dependent on readers' experience. As a result, subtle FCD lesions often eludes visual inspection during the radiological assessment [2], and patients are mistakenly diagnosed with MRI-negative epilepsy, missing opportunities for surgical treatment.

Previous studies have reported that a combined analysis of MRI and metabolic data from PET is more sensitive in detecting FCD type II [3, 4], and the hypometabolism of FCD in PET can help distinguish false-positive findings produced during the MRI post-processing [5]. Thus, visual assessment of PET-MRI co-registration has been routinely used in many epilepsy centers to detect FCD. In recent years, machine learning methods [6, 7, 8, 9] have also been applied to FCD detection. However, manually or automatically identifying lesions with subtle structural features or of tiny sizes accurately remains a challenge.

On the other hand, researches incorporating low-density electroencephalogram (EEG) data into automatic FCD detection are scarce. There are studies [10, 11, 12] employing high-density EEG to localize epileptogenic zones with electrophysiological source imaging (ESI) techniques. Nevertheless, as far as we know, high-density EEG data are not available in many epilepsy centers, and efforts can be made to incorporate low-density EEG data into automatic FCD detection.

ICCBR AI Track'24: Special Track on AI for Socio-Ecological Welfare at ICCBR2024, July 1, 2024, Mérida, Mexico
*Corresponding author.
zhengruifeng@zju.edu.cn (R. Zheng); chencong93@zju.edu.cn (C. Chen); huangkejie@zju.edu.cn (K. Huang)
0000-0003-3024-1510 (R. Zheng)

Given that the spacial resolution of low-density EEG is relatively limited, in this study, we propose a multi-modality solution which employed EEG, MRI, and PET to realize automatic FCD detection. Firstly, we followed our previous work [9], an automatic FCD detection algorithm combining MRI and PET data as inputs, to conduct preliminary FCD detection. Secondly, we utilized deep learning neural networks to conduct ESI. Specifically, we followed a framework offered by study[12] to generate training data through simulating electrical activities of a template brain; a continuous convolution network was utilized to process the EEG signals spatially; and a LSTM network was chosen to aggregate the features temporally. After that, the source imaging model was utilized to estimate the approximate sources of interictal epileptiform discharges (IED). In most cases, the sources of IED are close to or will overlap with the FCD lesions, so the IED source imaging results were adopted to improve the preliminary FCD detection results. Specifically, if the preliminary detection proposed multiple possible lesions, false-positive lesions outside the suspicious areas identified by the EEG data could be filtered out. Especially, when the preliminary FCD detection failed to locate the lesions, it could be guided by the IED source imaging results to generate more possible lesions in the suspicious areas.

Eight patients with MRI, PET, and identified IED were included in this study, and IED source imaging results overlapped with FCD lesions in seven (87.5%) cases. Among the seven cases, the average number of suspicious lesions output by the detection network decreased from 3 to 1.28 under the guidance of EEG, improving the specificity of the algorithm. Moreover, a tiny lesion with subtle structural features overlooked in the preliminary detection was located by the network after the introduction of EEG data. In summary, by combining low-density EEG data with MRI and PET data, our solution aims to improve FCD detection performance, especially in cases with weak structural and metabolic features.

2. Related work

In the past two to three years, representative studies on the localization of epileptic seizure onset zones using dense channel EEG data combined with ESI techniques include the following. Study [11] traced 76-channel EEG data and based on their experimental results, it was suggested that ictal epileptiform discharges during seizures are likely to have better source localization accuracy than IED during seizure-free intervals. Study [10] investigated the tracing of 76-channel EEG data and found that high-frequency oscillations occurring simultaneously with sharp waves contribute to characterizing the epileptic source area.

A concurrent study [13] indicated that relying solely on a single modality is difficult to achieve sufficient detection sensitivity and specificity, and thus integrated dense channel EEG data with MRI, PET, SPECT (single-photon emission computed tomography), and other data. Their dataset included 150 cases with negative MRI results or lesions that could not be confirmed by MRI alone, of which 32 cases were confirmed through surgical pathology. By combining different modalities in the experiments, this study concluded that the combination of IED tracing results, diffusion-weighted imaging from MRI, and nuclear medicine imaging achieved the highest accuracy.

The aforementioned studies utilized dense channel (76-channel) EEG data. However, to our knowledge, most epilepsy centers do not have equipment for collecting dense channel EEG data. Therefore, it is necessary to design multi-modal algorithms for localizing epileptic lesions in cases where only sparse channel (19-channel) EEG data is available.

Brain source localization algorithms can be classified into traditional algorithms and machine learning-based algorithms. Traditional electrophysiological source imaging methods include works such as [14, 15]. They treat the task of estimating brain's internal electrical activity from scalp EEG as an optimization problem. This optimization problem aims to find the sources inside the brain that best match the scalp EEG measurements. Since this optimization problem is ill-posed, conventional brain source imaging methods currently require prior assumptions to restrict the solution space: either using a small number of equivalent current dipole models to simulate brain activity [16, 17], or employing regularization terms in distributed source models based on prior knowledge of brain activity distribution [18]. However, considering the complexity of brain sources and brain networks, it is difficult to select

and customize prior regularization terms that fully express the properties of brain sources, thereby limiting the role of ESI in neuroscience research and clinical applications.

To overcome these limitations, a recent study [12] has approached brain source localization as a fitting problem based on a large amount of data, using deep learning algorithms for EEG source localization. However, the study did not utilize the positional information of different EEG electrodes. The values of electrode positions in space are continuous, making it difficult to represent them through voxelization. Studies [19], [20], and [21] proposed using deformable convolution kernels to replace high-resolution traditional discrete convolution kernels. Among them, the idea presented in [19] is to use multilayer perceptrons to approximate the weights of discrete convolution kernels in traditional convolutions. Study [21] defined kernel points located in space to place continuous convolution kernels and used linear rectification to control the distribution of kernel points in space. Previously, the authors proposed an adaptive kernel point continuous voxel convolution network to address this problem. The adaptive kernel points have two characteristics: they automatically distribute in space based on the input without the need for manually defining linear rectification functions, and they generate convolution weights based on the relative positions between input points and the kernel points.

3. Method

3.1. Clinical Case Acquisition

Eight patients were retrospectively included from the Second Affiliated Hospital of Zhejiang University School of Medicine. Interictal brain PET images were acquired using a PET/CT scanner (Biograph mCT, Siemens) at 40 minutes after intravenous injection of 18F-FDG (3.7 MBq/kg). FCD lesions were clearly identifiable on MRI with hindsight, and no other structural lesions were found. An experienced neurologist (C. C) manually drew the FCD lesion mask for each patient based on the 3D T1-weighted (T1W) images. The T2-weighted (T2W) and FLAIR images were also simultaneously reviewed to ensure accurate delineation of the dysplastic cortex. EEG electrodes were placed according to the International 10–20 system, and the data sampling rate was 500 Hz. IEDs were manually marked by (R. Z). All EEG data were passed through a 0.5-70 Hz band-pass filter, and the artificial components were removed using ICA analysis of EEGLAB before being fed into the model.

This study has been approved by the Medical Ethics Committee of the Second Affiliated Hospital, Zhejiang University School of Medicine. Written informed consent has been obtained from all patients or their guardians.

3.2. Preliminary FCD Detection

The procedure of preliminary FCD detection followed our previous work [9]. Here, we provide a brief introduction to the relevant content.

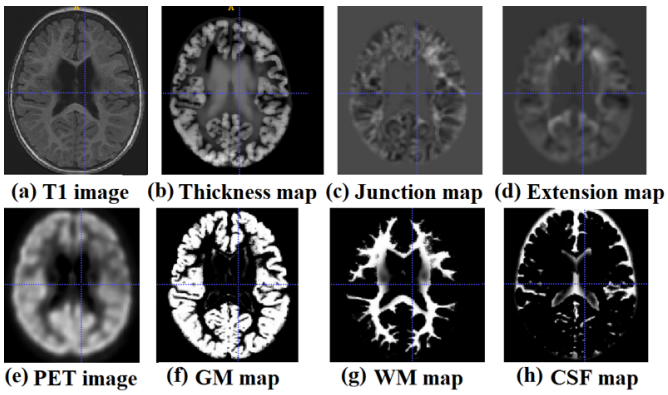

Figure 1: An example of all the input feature maps in a patient. GM: grey matter, WM: white matter, CSF: cerebrospinal fluid.

The detection neural network was trained and tested using MRI and PET data from 82 patients. The inputs of the network included structural features (junction, extension, and thickness maps extracted with MAP [22] tools), tissue segmentation results (gray matter (GM), white matter (WM), and cerebrospinal fluid (CSF)), and a metabolic feature (PET). All feature maps were registered to the MNI152 standard space, and regions such as the brainstem, diencephalon, basal ganglia, pituitary gland, and lateral ventricles were removed from the input feature maps since lesions do not appear in those areas. Figure 1 illustrates an example of all the filtered input feature maps.

The backbone network used was a 3D variant of U-Net and was deployed under the framework offered by nnU-Net [23] to reduce computational overhead. Additionally, the loss function was formed by combining Tversky loss [24] with Cross-entropy loss.

3.3. Deep Learning-Based IED Source Imaging

3.3.1. Training Data Generation

ESI is a crucial tool for noninvasively studying brain function and dysfunction. In this work, we employed deep learning neural networks for ESI to localize epileptogenic zones. This approach was chosen as it can be challenging for individuals without relevant training to select and optimize hyperparameters for conventional ESI solvers. Deep learning-based IED source imaging methods rely on a significant amount of brain dynamics and their corresponding EEG signals. We followed the framework proposed by Sun et al. [12] to generate training data by simulating electrical activities of a template brain.

Brain Dynamics Simulation For this study, all brain electrical activities were simulated on a template brain called fsaverage5, which is a T1-weighted MRI brain model. The template brain was processed using Freesurfer[25] to parcellate its cortical surface into 66 anatomical regions, and each anatomical region was further subdivided into smaller, approximately equal-sized regions to yield a total of 998 target regions of interest (ROIs). A connectivity analysis of the 998 ROIs was then conducted based on the study by Cammoun et al. [26] to a connectivity matrix. This connectivity matrix was subsequently input into TheVirtualBrain (TVB) platform [27] to simulate brain electrical activities. The biophysical model option in TVB was set to a neural mass model (NMM) [28], which has been demonstrated to replicate physiological brain characteristics by generating neural excitations and inhibitions.

Synthetic EEG Generation Our data collection devices had 19 scalp electrodes, and the electrodes were placed according to the International 10-20 system. Therefore, in Brainstorm [29], we set the EEG cap type as Colin27/Generic/10-20/19, and a lead field matrix was computed using openMEEG [30]. The role of the lead field matrix was to map the cortical activities to EEG electrode channels.

3.3.2. ESI Network Architectures

The objective of the ESI network was to estimate the brain activities of the 998 ROIs using signals from the 19 electrodes, as illustrated in Figure 2. The training data for the ESI network consisted of the EEG signals and their corresponding source cortical activities generated in the previous steps. Each input EEG sequence from each channel had a length of 500, representing 1-second EEG signals, based on a sampling rate of 500 Hz. The inputs $\in \mathbb{R}^{19\times500}$ were then preprocessed to ensure their values were distributed between -1.0 and 1.0. Specifically, the average value of a sequence was subtracted from the sequence values, followed by subtracting the average value of signals at the same time from the signals. Afterward, the inputs were divided by their maximum absolute value. Once preprocessed, the 19-channel EEG sequences needed to be aggregated spatially and temporally.

Spatial Aggregation In addition to the EEG signals from the 19 electrodes, the positions of these electrodes could also be utilized as inputs to organize the EEG signals spatially. However, the irregular format of electrode position information posed a challenge in effectively utilizing it. To address this

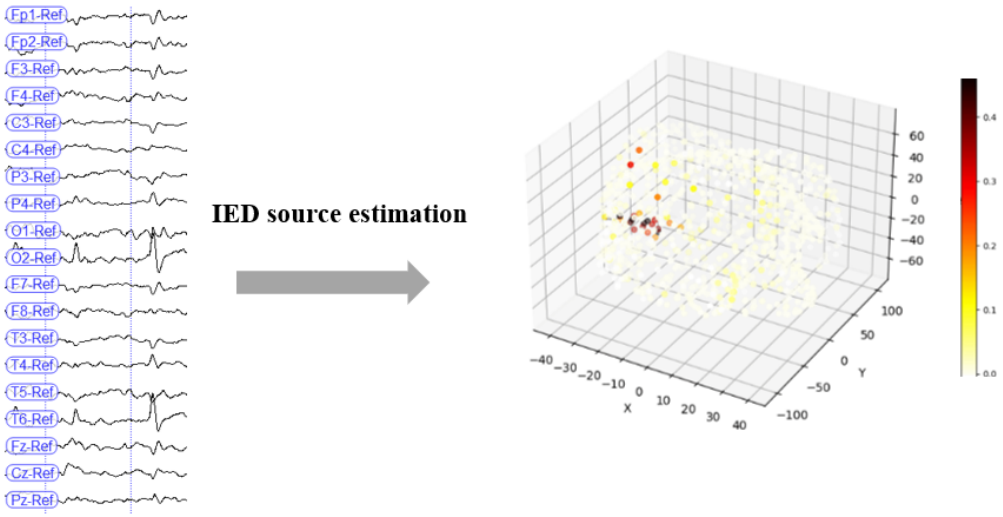

Figure 2: An example of IED source estimation.

issue, we explored and compared two different spatial aggregating schemes. The first approach involved extracting spatial features using a continuous convolution network [31], while the second approach encoded the position information and concatenated it with the electrode signals to form inputs. As far as our experiments showed, the former approach outperformed the latter, and thus, we selected it as our spatial aggregating solution.

The key idea of continuous convolution networks is to replace discrete (pixel or voxel-wise) convolution kernels typically used in traditional convolutional neural networks with continuous convolution kernels.

In our work, the continuous convolution network assumed that there were K convolution kernel points evenly distributed throughout the brain space. The positions of these kernel points were defined as $\{\widetilde{x}_k \mid k = 1, 2, ..., K\} \subset \mathcal{B}_r^3$, where K denoted the total number of kernel points, and $\mathcal{B}_r^3$ represented the brain space. Let x_i represent the coordinate of an electrode $\mathcal{P} \in \mathbb{R}^{N\times 3}$. By defining a function h to describe the distribution of kernel weights over $\mathcal{B}_r^3$, the kernel function g for any electrode $x_i \in \mathcal{B}_r^3$ could be expressed as:

$$g(x_i) = \sum_{k<K} h(x_i, \widetilde{x}_k) \tag{1}$$

Since the number of ROIs (998) was much larger than the number of electrodes (19), we set the number of kernel points to 256 and assigned input signals from the electrodes to the kernel points, rather than vice versa, in order to balance the disparity in quantity. Subsequently, the electrode signals could be aggregated to the kernel points as follows:

$$f_{kernel}(\widetilde{x}_k) = \sum_{n<N} h(x_n, \widetilde{x}_k) f_n \tag{2}$$

where N represented the number of electrodes, $f_i \in \mathbb{R}^{T\times 1}$ represented the EEG signals of the electrode, and T denoted the length of the signal.

Specifically, $h(x_n, \widetilde{x}_k)$ was approximated using a multi-layer perceptron (MLP). Each kernel had its corresponding MLP, enabling the projection of input signals to K kernel points through a set of K MLPs. Thus, Equation 2 could be reformulated as:

$$f_{kernel}(\widetilde{x}_k) = \sum_{n<N} MLP_k(x_n) f_n \tag{3}$$

The K MLPs had two main responsibilities: creating a set of K kernel points with implicit coordinates in the space and distributing electrode signals to the respective kernel points based on the relative positions between the electrodes and kernel points.

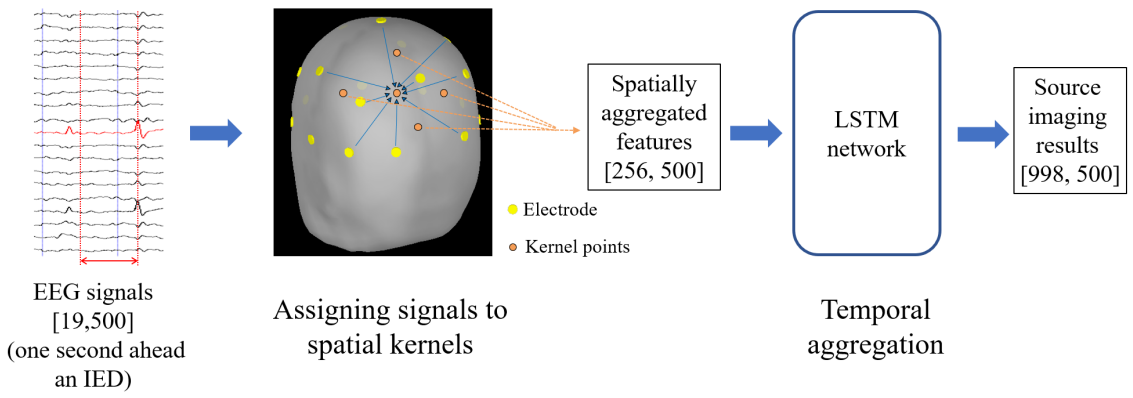

Figure 3: The overall data flow of IED source imaging

Temporal Aggregation Although the Transformer architecture has proven superior to RNNs in natural language processing, we employed LSTM (Long Short-Term Memory) [32] as our temporal aggregating network, similar to previous studies [12]. This decision was motivated by the computational efficiency advantages offered by LSTM over the Transformer. More importantly, the electrical activities within the brain at a given time point are predominantly influenced by preceding activities in close temporal proximity. Consequently, calculating attention between signals that are temporally distant would be redundant.

The input signals from the electrodes were first distributed to the kernel points. Subsequently, the spatially aggregated features were fed into the LSTM network to predict the electrical activities of the 998 ROIs. The overall data flow of IED source imaging is illustrated in Figure 3. Specifically, we utilized the mean square error between the network's estimated source cortical activities and the previously generated cortical activities as the loss function.

3.4. Multi-modality Fusion Strategy

In most cases, the sources of IED are located close to, or overlap with, FCD lesions, which makes it possible to utilize the IED source imaging results to improve the preliminary FCD detection outcomes. Additionally, the spatial resolution of low-density EEG is limited, and there may be discrepancies between the regions of IED and seizure onset zones [33]. Therefore, it is reasonable to employ IED source imaging results to conduct lobe-wise or hemisphere-wise guidance based on the quality of the source imaging results.

Specifically, if the preliminary detection suggests multiple possible lesions, false-positive lesions outside the suspicious areas identified by the EEG data can be filtered. Moreover, when the detection algorithm fails to locate the lesions, it can be guided by the IED source imaging results to generate additional possible lesions in the suspicious areas, thereby improving the lesion detection rate.

4. Experimental Results

4.1. IED Source Imaging Results

We conducted experiments to compare two spatial aggregating schemes: the continuous convolution network introduced in Section 3.3.2 and a Transformer network that encoded position information and concatenated it with electrode signals as inputs. The experimental results, presented in Table 1, demonstrated that the continuous convolution network achieved better performance. It could be attributed to the dimension expansion. By directly concatenating the signals and the electrode coordinates, the input dimension increased from one to three. However, it is important to note that the dimension representing the EEG signal values held greater significance compared to the other two

dimensions. Consequently, we selected the continuous convolution network as our spatial aggregating solution, which indirectly incorporated the position information.

Table 1
Experiment results of the two spatial aggregating schemes

Solution	Spatial aggregation method	Aggregation network	Mean square error
1	Continuous convolution kernels	Multi-layer perceptron	0.014
2	Concatenating coordinates with electrode signals	Transformer	0.060

We included eight patients with MRI, PET, and identified IED in this study. The IED source imaging results overlapped with FCD lesions in seven cases (87.5%), as shown in Figure 4. In the case that failed (Case 8), the source imaging result indicated strong electrical activities in the right occipital lobe, while the FCD lesion was actually located in the right temporal lobe, where only subtle activities were revealed. The source imaging results of Case 3 and Case 7 showed multiple source areas, and all of these possible source areas were considered as suspicious lesion areas.

4.2. EEG-Guided FCD Detection

Among the seven cases where the IED source imaging results overlapped with their FCD lesions, we were able to filter out false-positive lesions outside the suspicious areas identified by the EEG data. For example, in the preliminary detection results of Case 5, three possible lesions were identified, and the IED source imaging result indicated strong IED signals in the left frontal lobe. Therefore, we could filter out the possible lesions outside the suspicious lobe and obtain the final predicted lesion position, as shown in Figure 5. Moreover, when the detection algorithm failed to locate the lesions, we could use the IED source imaging results to generate additional possible lesions in the suspicious areas.

Table 2
Detection results before and after the guidance of EEG data.

Case ID	IED source imaging areas	without EEG guidance		with EEG guidance	
		Suspicious lesions number	Detection result	Suspicious lesions number	Detection result
1	2	4	Success	1	Success
2	1	2(14*)	Fail	0(2*)	Fail/Success*
3	1	3	Success	3	Success
4	1	3	Success	1	Success
5	1	2	Success	1	Success
6	2	2	Success	1	Success
7	2	5	Success	2	Success
Mean	1.43	3	-	1.28	-

*: The results of a high-sensitivity version of the detection network

The detection results of the seven patients before and after the guidance of the EEG data are listed in Table 2. The average number of suspicious lesions output by the detection network decreased from 3 to 1.28 under the guidance of EEG, thus improving the specificity of the algorithm. Notably, in Case 2, a small lesion with subtle structural features was initially overlooked in the preliminary detection but successfully identified after incorporating the EEG data. Specifically, despite the preliminary detection did not detect the lesion, the source imaging result indicated the right occipital lobe as a suspicious area. Consequently, the detection network was adjusted to propose additional possible lesions. Out of the 14 possible lesions suggested by the tuned network, only two were situated within the suspicious lobe, and one of them overlapped with the ground truth lesion, thus effectively uncovering the FCD lesion.

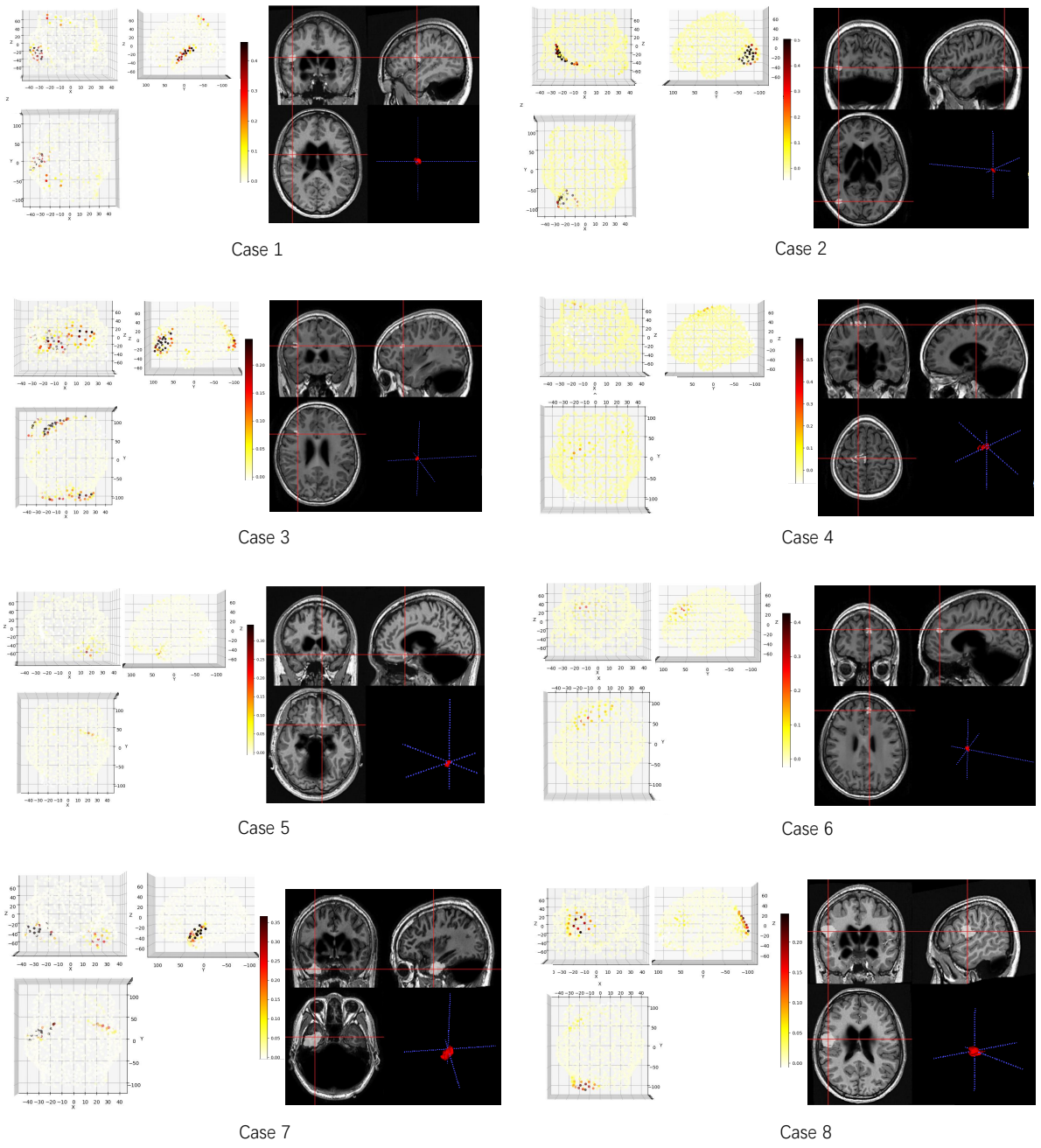

Figure 4: The IED source imaging results of all the cases. Left: Sources of IEDs estimated by the network, where the values indicate the relative strength of electrical activities in the ROIs. Right: Lesions marked by an experienced neurologist.

5. Discussion

5.1. Data Modalities

High-density EEG provides higher spatial resolution than low-density EEG. However, high-density EEG devices are not widely available in epilepsy centers. Besides, a study [11] reported that the values of ictal recordings over interictal recordings might be overlooked. Nevertheless, the ictal recordings are much scarcer and often unavailable due to limited EEG recording time. Therefore, our proposed solution aims to enhance the performance of focal cortical dysplasia detection in scenarios where both high-density EEG sensors and ictal EEG recordings are unavailable. This approach offers advantages in terms of data accessibility.

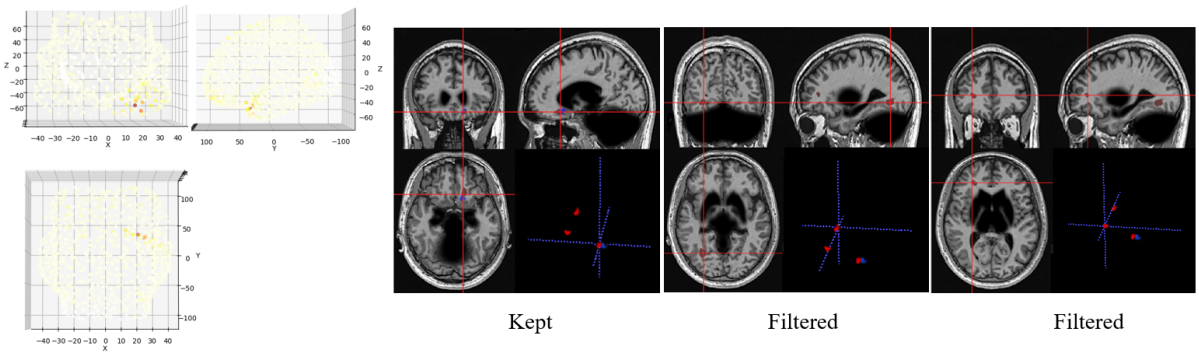

(a) IED source results (b) Suspicious lesions (red) and the ground truth lesion (blue)

Figure 5: Possible lesions outside the suspicious lope were filtered.

5.2. Limitations

Due to the limited number of identified IED recordings, our study only included eight patients. To validate the generality of our solution, further research with a larger sample size is necessary.

We only implemented a deep learning-based IED source imaging scheme and did not explore traditional IED source imaging methods. Additionally, the structural differences between patients' brains and the template brain are to introduce deviations which cannot be omitted. Therefore, the source imaging solution in our work could be further optimized or replaced by other methods.

6. Conclusions

In this study, we propose a multi-modality solution that utilizes an additional modality derived from EEG to guide the detection of type II FCD. We employed low-density EEG data to estimate the sources of IED using a deep learning-based neural network, and the source imaging results showed an overlap with FCD lesions in 87.5% of the cases. Among the seven successful cases, the average number of suspicious lesions output by the detection network decreased from 3 to 1.28 under the guidance of EEG. Furthermore, the network successfully located a small lesion with subtle structural features that had been overlooked in the preliminary detection. By combining low-density EEG data with MRI and PET data, our solution aims to improve FCD detection performance, particularly in cases with weak structural and metabolic features.

References

[1] J. T. Lerner, N. Salamon, J. S. Hauptman, T. R. Velasco, M. Hemb, J. Y. Wu, R. Sankar, W. Donald Shields, J. Engel Jr, I. Fried, et al., Assessment and surgical outcomes for mild type i and severe type ii cortical dysplasia: a critical review and the ucla experience, Epilepsia 50 (2009) 1310–1335.

[2] P. Besson, F. Andermann, F. Dubeau, A. Bernasconi, Small focal cortical dysplasia lesions are located at the bottom of a deep sulcus, Brain 131 (2008) 3246–3255.

[3] Y. Lin, Y.-H. D. Fang, G. Wu, S. E. Jones, R. A. Prayson, A. N. Moosa, M. Overmyer, J. Bena, M. Larvie, W. Bingaman, et al., Quantitative positron emission tomography–guided magnetic resonance imaging postprocessing in magnetic resonance imaging–negative epilepsies, Epilepsia 59 (2018) 1583–1594.

[4] J.-J. Mo, J.-G. Zhang, W.-L. Li, C. Chen, N.-J. Zhou, W.-H. Hu, C. Zhang, Y. Wang, X. Wang, C. Liu, et al., Clinical value of machine learning in the automated detection of focal cortical dysplasia using quantitative multimodal surface-based features, Frontiers in neuroscience 12 (2019) 1008.

[5] C. Chen, J.-J. Xie, F. Ding, Y.-S. Jiang, B. Jin, S. Wang, Y. Ding, H. Li, B. Jiang, J.-M. Zhu, et al.,

7t mri with post-processing for the presurgical evaluation of pharmacoresistant focal epilepsy, Therapeutic Advances in Neurological Disorders 14 (2021) 17562864211021181.

[6] K. Snyder, E. P. Whitehead, W. H. Theodore, K. A. Zaghloul, S. J. Inati, S. K. Inati, Distinguishing type ii focal cortical dysplasias from normal cortex: a novel normative modeling approach, NeuroImage: Clinical 30 (2021) 102565.

[7] B. David, J. Kröll-Seger, F. Schuch, J. Wagner, J. Wellmer, F. Woermann, B. Oehl, W. Van Paesschen, T. Breyer, A. Becker, et al., External validation of automated focal cortical dysplasia detection using morphometric analysis, Epilepsia 62 (2021) 1005–1021.

[8] I. S. Fernández, E. Yang, M. Amengual-Gual, C. B. Aguilar, P. C. Prieto, J. M. Peters, Convolutional neural networks to identify malformations of cortical development: A feasibility study, Seizure 91 (2021) 81–90.

[9] R. Zheng, R. Chen, C. Chen, Y. Yang, Y. Ge, L. Ye, P. Miao, B. Jin, H. Li, J. Zhu, et al., Automated detection of focal cortical dysplasia based on magnetic resonance imaging and positron emission tomography, Seizure: European Journal of Epilepsy (2024).

[10] Z. Cai, A. Sohrabpour, H. Jiang, S. Ye, B. Joseph, B. H. Brinkmann, G. A. Worrell, B. He, Noninvasive high-frequency oscillations riding spikes delineates epileptogenic sources, Proceedings of the National Academy of Sciences 118 (2021).

[11] S. Ye, L. Yang, Y. Lu, M. T. Kucewicz, B. Brinkmann, C. Nelson, A. Sohrabpour, G. A. Worrell, B. He, Contribution of ictal source imaging for localizing seizure onset zone in patients with focal epilepsy, Neurology 96 (2021) e366–e375.

[12] R. Sun, A. Sohrabpour, G. A. Worrell, B. He, Deep neural networks constrained by neural mass models improve electrophysiological source imaging of spatiotemporal brain dynamics, Proceedings of the National Academy of Sciences 119 (2022) e2201128119.

[13] R. Mareček, P. Říha, M. Bartoňová, M. Kojan, M. Lamoš, M. Gajdoš, L. Vojtíšek, M. Mikl, M. Bartoň, I. Doležalová, et al., Automated fusion of multimodal imaging data for identifying epileptogenic lesions in patients with inconclusive magnetic resonance imaging, Human Brain Mapping 42 (2021) 2921–2930.

[14] B. He, A. Sohrabpour, E. Brown, Z. Liu, Electrophysiological source imaging: a noninvasive window to brain dynamics, Annual review of biomedical engineering 20 (2018) 171–196.

[15] J. Gross, J. Kujala, M. Hämäläinen, L. Timmermann, A. Schnitzler, R. Salmelin, Dynamic imaging of coherent sources: studying neural interactions in the human brain, Proceedings of the National Academy of Sciences 98 (2001) 694–699.

[16] B. He, T. Musha, Y. Okamoto, S. Homma, Y. Nakajima, T. Sato, Electric dipole tracing in the brain by means of the boundary element method and its accuracy, IEEE Transactions on Biomedical Engineering (1987) 406–414.

[17] M. Scherg, D. Von Cramon, Evoked dipole source potentials of the human auditory cortex, Electroencephalography and Clinical Neurophysiology/Evoked Potentials Section 65 (1986) 344–360.

[18] R. D. Pascual-Marqui, et al., Standardized low-resolution brain electromagnetic tomography (sloreta): technical details, Methods Find Exp Clin Pharmacol 24 (2002) 5–12.

[19] W. Wu, Z. Qi, L. Fuxin, Pointconv: Deep convolutional networks on 3d point clouds, in: Proceedings of the IEEE/CVF Conference on Computer Vision and Pattern Recognition, 2019, pp. 9621–9630.

[20] A. Boulch, Convpoint: Continuous convolutions for point cloud processing, Computers & Graphics 88 (2020) 24–34.

[21] H. Thomas, C. R. Qi, J.-E. Deschaud, B. Marcotegui, F. Goulette, L. J. Guibas, Kpconv: Flexible and deformable convolution for point clouds, in: Proceedings of the IEEE/CVF international conference on computer vision, 2019, pp. 6411–6420.

[22] H.-J. Huppertz, C. Grimm, S. Fauser, J. Kassubek, I. Mader, A. Hochmuth, J. Spreer, A. Schulze-Bonhage, Enhanced visualization of blurred gray–white matter junctions in focal cortical dysplasia by voxel-based 3d mri analysis, Epilepsy research 67 (2005) 35–50.

[23] F. Isensee, P. F. Jaeger, S. A. Kohl, J. Petersen, K. H. Maier-Hein, nnu-net: a self-configuring method for deep learning-based biomedical image segmentation, Nature methods 18 (2021) 203–211.

[24] S. S. M. Salehi, D. Erdogmus, A. Gholipour, Tversky loss function for image segmentation using 3d fully convolutional deep networks, in: International workshop on machine learning in medical imaging, Springer, 2017, pp. 379–387.
[25] B. Fischl, Freesurfer, Neuroimage 62 (2012) 774–781.
[26] L. Cammoun, X. Gigandet, D. Meskaldji, J. P. Thiran, O. Sporns, K. Q. Do, P. Maeder, R. Meuli, P. Hagmann, Mapping the human connectome at multiple scales with diffusion spectrum mri, Journal of neuroscience methods 203 (2012) 386–397.
[27] P. Sanz Leon, S. A. Knock, M. M. Woodman, L. Domide, J. Mersmann, A. R. McIntosh, V. Jirsa, The virtual brain: a simulator of primate brain network dynamics, Frontiers in neuroinformatics 7 (2013) 10.
[28] M. Breakspear, Dynamic models of large-scale brain activity, Nature neuroscience 20 (2017) 340–352.
[29] F. Tadel, S. Baillet, J. C. Mosher, D. Pantazis, R. M. Leahy, Brainstorm: a user-friendly application for meg/eeg analysis, Computational intelligence and neuroscience 2011 (2011) 1–13.
[30] A. Gramfort, T. Papadopoulo, E. Olivi, M. Clerc, Openmeeg: opensource software for quasistatic bioelectromagnetics, Biomedical engineering online 9 (2010) 1–20.
[31] R. Zheng, K. Huang, H. Shen, L. Ma, Continuous volumetric convolution network with self-learning kernels for point clouds, IEEE Transactions on Consumer Electronics 69 (2022) 148–155.
[32] S. Hochreiter, J. Schmidhuber, Long short-term memory, Neural computation 9 (1997) 1735–1780.
[33] E. D. Marsh, B. Peltzer, M. W. Brown III, C. Wusthoff, P. B. Storm Jr, B. Litt, B. E. Porter, Interictal eeg spikes identify the region of electrographic seizure onset in some, but not all, pediatric epilepsy patients, Epilepsia 51 (2010) 592–601.